Hybrid Polarimetric GPR Calibration and Elongated Object Orientation Estimation

Hai Liu , *Member, IEEE*, Xiaoyun Huang , Feng Han , *Member, IEEE*, Jie Cui ,
Billie F. Spencer, and Xiongyao Xie

Abstract—Ground penetrating radar (GPR) has been widely applied to the detection of subsurface elongated targets, such as underground pipes, concrete rebars, and subsurface fractures. The orientation angle of a subsurface elongated target can hardly be delineated by a commercial single-polarization GPR system. In this paper, a hybrid dual-polarimetric GPR system, which consists of a circularly polarized transmitting antenna and two linearly polarized receiving antenna, is employed to detect buried elongated objects. A polarimetric calibration experiment using a gridded trihedral is carried out to correct the imbalances and cross talk between the two receiving channels. A full-polarimetric scattering matrix is extracted from the double-channel GPR signals reflected from a buried elongated object. An improved Alford rotation method is proposed to estimate the orientation angle of the elongated object from the extracted scattering matrix, and its accuracy is validated by a numerical test. A laboratory experiment was further conducted to detect five metal rebar buried in dry sand at different orientation angle relative to the GPR scan direction. The maximum relative error of the estimated angles of the buried rebars in the migrated GPR images is less than 5%. It is concluded that radar polarimetry can provide not only richer information than single-polarization GPR, but also a reliable approach for orientation estimation of a subsurface elongated object.

Index Terms—Azimuth estimation, ground penetrating radar (GPR), hybrid polarization, subsurface elongated target.

I. Introduction

GROUND penetrating radar (GPR) has been widely applied to detecting and imaging of subsurface elongated targets, such as buried pipes, cables, concrete rebars, and subsurface fractures [1]–[4]. Generally, a commercial GPR system employs a pair of dipole or bowtie antennas, which transmits and receives nearly linearly polarized electromagnetic waves. Thus, the reflection signal from the subsurface elongated object is sensitive to its orientation direction with respect to the polarization direction of the transmitting and receiving antennas [5], [6]. When the antenna polarization direction is perpendicular to the orientation of the elongated object, the target reflection is weak or even undetectable [7], [8]. To increase the capability of GPR for detecting a subsurface elongated object, radar polarimetry has been widely explored. A multicomponent GPR dataset can be acquired by a repeated survey using different combination of bistatic antenna arrangement [4], [9]. To increase the coherency of the multicomponent GPR data, a dual-polarization GPR system, which consists of two couples of dipole antennas at orthogonal polarization, has been applied to elongated target detection [10]. Full polarimetric GPR systems, which enable the measurement of the four components of the polarimetric scattering matrix, have also been developed for subsurface target detection [6], [11]. A full polarimetric GPR system can not only improve the target detection accuracy [12], but also classify the geometric information of the subsurface target [9], [13]. However, a high-speed coaxial switch is required in a full-polarimetric GPR system, so that the system complexity and the data acquisition time are increased. In our previous work, a hybrid dual-polarization GPR system, which consists of a circularly polarized transmitting antenna and two linearly polarized receiving antennas, has been proposed for the detection of subsurface elongated objects [2]. This system can simultaneously record the dual-channel GPR data, from which the scattering matrix of the subsurface reflection can be extracted. In this paper, we further explore the potential of this GPR system for estimating the orientation angle of a buried elongated object.

The orientation of a subsurface elongated object can be readily estimated from multiple parallel GPR profiles recorded on ground surface [14]. However, this method drastically increase the data acquisition time and can yield inaccurate results when multiple linear objects are interlaced in subsurface. In a harsh field environment, it is not easy to acquire multiple parallel GPR profiles. Various methods have been proposed to classify and estimate the orientation angle of a subsurface elongated target from the scattering matrix extracted from the polarimetric GPR signal. The linearity factor estimated from the eigenvalues of the scattering matrix can be used to classify rotationally symmetric and elongated objects [11], [15]. An elongated target has a preferential scattering axis that coincides with its long axis [15].

The strike direction of a subsurface fracture can be estimated by minimizing the energy of the cross-polarized components, which is realized by zeroing the derivative of the energy in the cross-polarization channel [16]. However, to mitigate the influence of noise, Capizzi and Cosentino estimate the orientation angle by maximizing the energy in the two cross-polarization channels, and the result is obtained from an average of two angles [17]. To make the angle estimation more stable, the Frobenius norm of the scattering matrix is used as a criterion for selection of strong amplitudes in the reflection hyperbola [8]. However, the orientation angle estimated by these algorithms has an ambiguity of 90° [9].

Calibration has to be applied to a polarimetric radar system to ensure that the scattering behavior is faithfully represented. The purpose of a polarimetric calibration is to estimate and correct the imbalances and cross talk between the channels delivering different polarimetric responses. It usually consists of two steps. The first step is to establish a suitable distortion model and the second step is to estimate the imbalance and cross-talk parameters by comparing observed data to the theoretical scattering matrix from specially made corner reflectors [18]. Various methods have been proposed for calibrating full-polarimetric radar systems [18], [19], as well as hybrid polarimetric synthetic aperture radar (SAR) systems in the circular transmitting and linear receiving mode [20], [21], which have a similar architecture with our hybrid GPR system. These polarimetric calibration methods are defined in the frequency domain. For an ultra-wideband radar system like GPR, it is convenient to evaluate the calibration parameters in the time domain [22].

In this paper, we calibrate the hybrid dual-polarization GPR system using a gridded trihedral and extract the scattering matrix of the subsurface reflection from the recorded complex time domain signals in two receiving channels. Then, we extend the algorithm in [8] to estimate the orientation angle of a buried elongated object using the Alford rotation method. This paper is organized as follows. In Section II, we introduce the hybrid dual-polarization GPR system and the calibration method. Section III presents the algorithm for orientation angle estimation. The results of a numerical validation of the algorithm and a laboratory experiment are given in Sections IV and V, and the conclusion is presented in Section VI.

II. HYBRID DUAL-POLARIZATION GPR SYSTEM

A. Hybrid Dual-Polarization GPR System

Fig. 1 shows the hybrid dual-polarization GPR antenna array, which consists of a right-hand planar spiral antenna for transmitting and two orthogonally oriented Vivaldi antennas for receiving radar signals. Based on a vector network analyzer (VNA), a stepped-frequency GPR system has been established, and it records GPR signal at 596 frequency samples from 50 MHz to 6 GHz in the frequency domain. Constrained by the employed antennas, the effective frequency bandwidth is from 1.2 to 4.0 GHz [2]. Utilizing a coaxial switch, two GPR profiles can be recorded in the two receiving channels by a single scan over a survey line.

Ideally, the circularly polarized electromagnetic waves radiated by the spiral transmitting antenna, i.e., the incident waves, can be decomposed into two linear components, which are
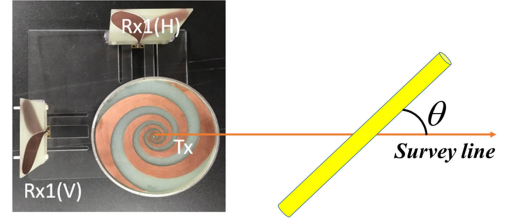

Fig. 1. Manufactured hybrid dual-polarization GPR antenna array.

orthogonal to each other and have the same magnitude but 90° phase difference, as given by

$$\mathbf{E_i} = \begin{bmatrix} T_H \\ T_V \end{bmatrix} = \frac{1}{\sqrt{2}} \begin{bmatrix} 1 \\ -j \end{bmatrix} E_R \qquad (1)$$

where E_R is the amplitude of the radiated right-hand circularly polarized electromagnetic waves, T_H and T_V are the decomposed components in the horizontal and vertical directions, respectively.

The scattered signals observed by two ideal probes oriented in the horizontal and vertical directions can be expressed using the scattering matrix, as given by

$$\begin{bmatrix} M_{RH} \\ M_{RV} \end{bmatrix} = \mathbf{S}\mathbf{E_i} = \begin{bmatrix} S_{HH} & S_{HV} \\ S_{VH} & S_{VV} \end{bmatrix} \mathbf{E_i}. \qquad (2)$$

Substituting (1) into (2), the scattered signal recorded by an ideal hybrid polarimetric GPR system can be expressed as follows:

$$\begin{bmatrix} M_{RH} \\ M_{RV} \end{bmatrix} = \frac{1}{\sqrt{2}} \begin{bmatrix} S_{HH} & S_{HV} \\ S_{VH} & S_{VV} \end{bmatrix} \begin{bmatrix} 1 \\ -j \end{bmatrix} E_R. \qquad (3)$$

A complex reflection signal in each polarization channel can be obtained from the data recorded by VNA through inverse Fourier transformation. Thus, we can calculate the scattering matrix from the amplitude of the reflection signals in the time domain acquired by the hybrid polarimetric GPR system. In reality, an ideal antenna does not exist. Thus, system errors, such as channel imbalance and cross talk, are unavoidable. Ignoring noise, the measured radar signals in the two linear polarization channels can be expressed as [20]

$$\begin{bmatrix} M_{RH} \\ M_{RV} \end{bmatrix} = \frac{1}{\sqrt{2}} \begin{bmatrix} 1 & \delta_2 \\ \delta_1 & f \end{bmatrix} \begin{bmatrix} S_{HH} & S_{HV} \\ S_{VH} & S_{VV} \end{bmatrix} \begin{bmatrix} 1 \\ -j \end{bmatrix} T_R \qquad (4)$$

where M_{RH} and M_{RV} are the analytical reflection signals recorded in two receiving channels by VNA, S_{HH}, S_{HV}, S_{VH} and S_{VV} are the full-polarimetric components of the scattering matrix, δ_1, δ_2 are the cross-talk parameters, and f is the channel imbalance.

B. Polarimetric Calibration

A polarimetric calibration method using a gridded trihedral has been successfully applied to a hybrid polarimetric SAR system [20]. We extend this method to calibrate our hybrid dual-polarization GPR antenna array in the time domain. The geometry of the gridded trihedral calibrator is shown in Fig. 2. Let the radar illuminate electromagnetic waves towards the
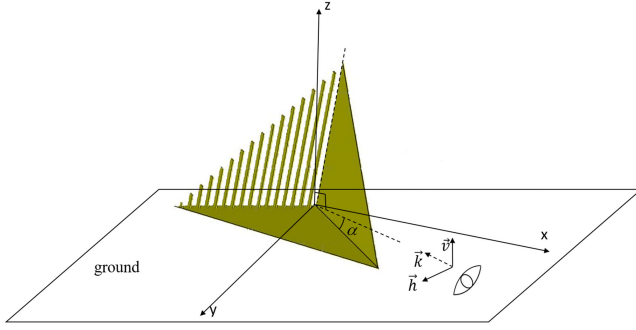
Fig. 2. Geometry of the gridded trihedral for calibrating the hybrid dual-polarization GPR antenna array.

corner of the trihedral, α and β respectively denote the yaw and roll relative to the flight direction of radar waves reflected from the trihedral back to the radar. Assuming the antennas under test are in the far field, the scattering matrix of the GPR reflection from the gridded trihedral is represented by

$$S_{gt} = \begin{bmatrix} \cos^2 \beta & -\sin \alpha \cos \alpha \sin \beta \\ -\sin \alpha \cos \alpha \sin \beta & \cos^2 \alpha \cdot \sin^2 \beta \end{bmatrix}. \quad (5)$$

Let S_{gt1} and S_{gt2} denote the scattering matrices of the gridded trihedral calibrator under two special conditions, i.e., when $\beta = 90°$, $\alpha = 0°$ (horizontal grid) and $\beta = 0°$, $\alpha = 0°$(vertical grid) respectively, and they can be given by [23]

$$S_{gt1} = \begin{bmatrix} 0 & 0 \\ 0 & 1 \end{bmatrix} \quad S_{gt2} = \begin{bmatrix} 1 & 0 \\ 0 & 0 \end{bmatrix}. \quad (6)$$

By substituting (6) into (4), we obtain the channel imbalance and the cross talks as

$$\delta_1 = \frac{M_{RV}^{gt1}}{M_{RH}^{gt1}} \qquad \delta_2 = j\frac{M_{RH}^{gt2}}{M_{RH}^{gt1}}$$

$$T_R = \sqrt{2}M_{RH}^{gt1} \qquad f = j\frac{M_{RV}^{gt2}}{M_{RH}^{gt1}}. \quad (7)$$

M_{RV}^{gt1}, M_{RH}^{gt1}, M_{RV}^{gt2}, and M_{RH}^{gt2} are the measured scattering vectors at the arriving time from the horizontal ($gt1$) and vertical ($gt2$) gridded trihedral calibrator received by the two orthogonal linearly polarized (H and V) channels. The arriving time is evaluated by the maximum amplitude of signal reflected from the horizontal gridded trihedral in the H channel.

Substituting (7) in (4), the calibrated scattering vectors can be obtained

$$\begin{bmatrix} M'_{RH} \\ M'_{RV} \end{bmatrix} = \begin{bmatrix} S_{HH} - jS_{HV} \\ S_{VH} - jS_{VV} \end{bmatrix} = \frac{\sqrt{2}}{T_R} \begin{bmatrix} M_{RH} \\ M_{RV} \end{bmatrix} \begin{bmatrix} 1 & \delta_2 \\ \delta_1 & f \end{bmatrix}^{-1} \quad (8)$$

where M'_{RH} and M'_{RV} are the calibrated scattering vectors. Therefore, we obtain the calibrated scattering matrix of the GPR signal reflected from the subsurface target as

$$\mathbf{S} = \begin{bmatrix} S_{HH} & S_{HV} \\ S_{VH} & S_{VV} \end{bmatrix} = \begin{bmatrix} real(M_{RH}) & -imag(M'_{RH}) \\ real(M'_{RV}) & -imag(M'_{RV}) \end{bmatrix}. \quad (9)$$

III. ORIENTATION ANGLE ESTIMATION

A. Orientation Estimation by Alford Rotation

The Alford rotation transformation [24] is applied to the extracted scattering matrix of the reflected GPR signal to estimate the orientation of the buried elongated target, and its expression is given by

$$\mathbf{E} = \mathbf{RSR}^T, \text{ where} \quad (10)$$

$$\mathbf{R} = \begin{bmatrix} \cos \theta & \sin \theta \\ -\sin \theta & \cos \theta \end{bmatrix} \quad (11)$$

where θ is the anti-clockwise angle from the orientation of the GPR antenna in the horizontal polarization channel (parallel to the survey line) to the orientation of the buried elongated object, as illustrated in Fig. 1. The range of θ is from 0° to 180°.

The meaning of the Alford rotation transformation is a mathematical rotation of the measurement frame to investigate the target's response as a function of the polarization direction. After collecting GPR data in just four different polarimetric configuration, i.e., HH, HV, VH, and VV, we can calculate the GPR response for any orientation angle of the antenna. The reflection signals in four different polarization channels after the Alford rotation transformation can be represented by

$$E_{HH} = \cos^2 \theta \cdot S_{HH} + \sin^2 \theta \cdot S_{VV} + 0.5 \sin 2\theta \cdot (S_{VH} + S_{HV})$$

$$E_{HV} = \cos^2 \theta \cdot S_{HV} - \sin^2 \theta \cdot S_{VH} + 0.5 \sin 2\theta \cdot (S_{VV} - S_{HH})$$

$$E_{VH} = \cos^2 \theta \cdot S_{VH} - \sin^2 \theta \cdot S_{HV} + 0.5 \sin 2\theta \cdot (S_{VV} - S_{HH})$$

$$E_{VV} = \cos^2 \theta \cdot S_{VV} + \sin^2 \theta \cdot S_{HH} - 0.5 \sin 2\theta \cdot (S_{VH} + S_{HV}). \quad (12)$$

Take derivative of E_{HH} with respect to θ

$$\frac{d(E_{HH})}{d\theta} = (S_{VV} - S_{HH}) \sin 2\theta + (S_{VH} + S_{HV}) \cos 2\theta. \quad (13)$$

Making zero the derivative above, the reflection amplitude in the co-polarized channel reaches to maximum, and we can estimate the angle between the antenna and target orientation by [8]

$$\theta = \frac{1}{2} \arctan\left(\frac{S_{HV} + S_{VH}}{S_{HH} - S_{VV}}\right). \quad (14)$$

It is noted that the estimated orientation angle above ranges from –45° to 45°, and has an ambiguity of 90°. It is proved that the reflection amplitude of the cross-pol component is negative when the anti-clockwise angle from the orientation of the survey line to the orientation of the elongated target is in the range of 0°–90°, and positive in the range of 90°–180° [9]. Making use of this property, we can eliminate the ambiguity and estimate the orientation angle of the target relative to the survey direction by

$$\begin{cases} \theta_{tar} = \theta, & (\theta > 0, S_{VH} < 0) \\ \theta_{tar} = \theta + \pi, & (\theta < 0, S_{VH} > 0) \\ \theta_{tar} = \theta + \frac{\pi}{2}, & (others). \end{cases} \quad (15)$$

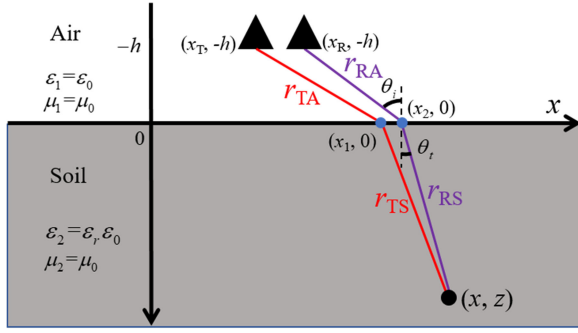Therefore, the range of θ_{tar} is from 0° to 180°.

Fig. 3.   Geometry configuration for the bi-static radar migration.

B. Migration Algorithm

Migration, also called SAR processing, of a GPR image can reconstruct the geometric shape, and benefit the detection and location of a subsurface object. Thus, we apply a simple back projection (BP) algorithm to the recorded GPR image before estimating the orientation angle of the buried elongated object. Since the employed hybrid GPR antenna array operates in an off-ground mode, a half-space model is used for the BP migration, as shown in Fig. 3. The GPR antennas are simplified as a point source at their phase centers. For the planar spiral transmitting antenna, its phase center locates at the feeding point. For the Vivaldi receiving antenna, its phase center is measured at the 20 mm away from the antenna opening end on the symmetric axis [25]. The two-way travel-time of a subsurface reflection includes two parts, i.e., the downward and the upward ray paths. For each ray path, a refraction occurs on the ground surface, and it satisfies Snell's law by

$$\frac{\sin \theta_i}{\sin \theta_t} = \sqrt{\varepsilon_r} \tag{16}$$

where ε_r is the relative permittivity of the subsurface medium. A direct solution of the refraction point is not easy, since it is quartic equation [26]. Therefore, we calculate the refraction point of each ray path by an iterative method. The two-way travel-time of the signal reflected from the subsurface imaging point (x, z) in the ith GPR trace can be calculated by

$$\tau_i(x, z) = \frac{r_{\text{TA}} + r_{\text{RA}}}{c} + \varepsilon_r \frac{r_{\text{TS}} + r_{\text{RS}}}{c} \tag{17}$$

where c is the velocity of electromagnetic waves in vacuum, r_{TA} and r_{RA} are lengths of the downward and upward paths in air, respectively, and r_{TS} and r_{RS} are those in the subsurface medium. The reconstructed GPR image can be obtained by

$$I(x, z) = \sum_{i}^{N} A_i(\tau_i(x, z)) \tag{18}$$

where $A_i(\tau)$ is the amplitude of the ith recorded GPR signal at τ, and N is the total number of the GPR traces along the survey line.
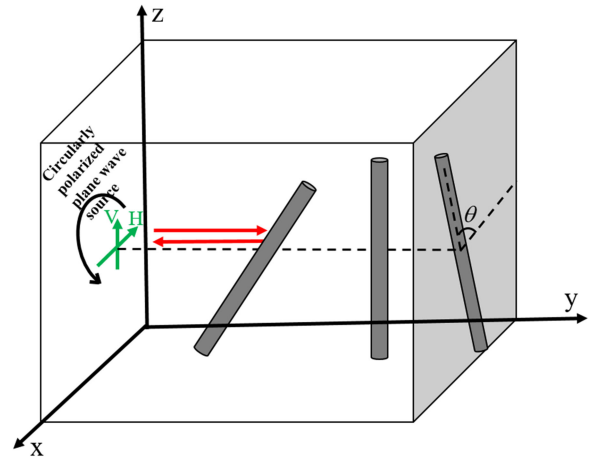

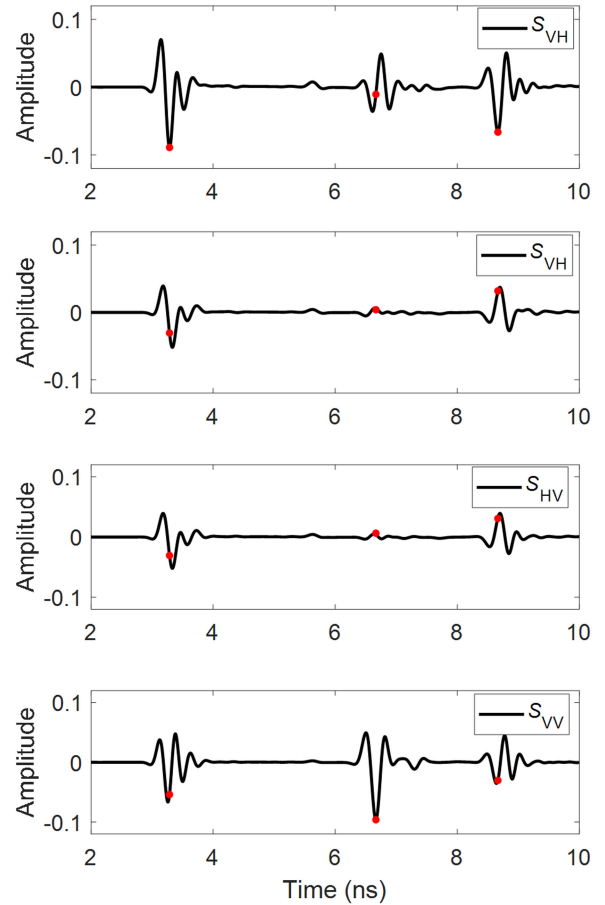Fig. 4.   3-D schematic view of the numerical model.

Fig. 5.   Decomposed GPR signals in four different polarization channels from the simulated two traces. The arrival time of the reflected signal is indicated by a red point.

IV. NUMERICAL VALIDATION

A numerical simulation is conducted to validate the accuracy of the proposed algorithm for orientation estimation using the Alford rotation transformation. The model is shown in Fig. 4. Three rebars with a diameter of 16 mm are oriented at 30°, 90°, and 150° with respect to the $-x$-axis in the xz plane, respectively. The distances from the source to the three rebars are 40, 90,

and 120 cm, respectively. The background medium is air, and the targets are illuminated by a circularly polarized plane wave source. Two probes respectively in the x (H) and z (V) directions record the reflected signals from the metal pipes. Using (7), the recorded GPR signals can be decomposed into four traces in different polarization channels, which are shown in Fig. 5. We can find the signals in the two cross-pol channels, i.e., S_{HV} and S_{VH}, are the same due to the reciprocity. The arrival times of signals reflected from the three rebars are picked from the point of maximum absolute amplitude, and they are about 3.3, 6.7, and 8.7 ns, respectively. The amplitude of the reflected signal in each channel is picked from the time of arrival and a polarimetric scattering matrix is obtained from each reflection.

Fig. 6 shows the polar diagram of the amplitudes of three reflection signals in four different polarization channels after the Alford rotation transformation of the scattering matrix. We can find that the co-pol amplitudes are related with $E_{XX}(\theta) = E_{YY}(\theta + 90°)$, and that the cross-pol amplitudes are the same due to the reciprocity principle. The small visible difference between the cross-pol amplitudes is caused by the numerical dispersion error. The orientation angles of the three pipes, which maximize the HH component as indicated by an arrow, are estimated to be 30.1°, 92.5°, and 149.9°, indicating a high accuracy. The relative large error observed for the 90° rebar is caused by the numerical dispersion error, which leads to a small difference between the signals in the two cross-pol channels.

V. LABORATORY EXPERIMENTS

First, we conducted an experiment in an anechoic chamber to calibrate the hybrid GPR antenna array using a gridded trihedral, as shown in Fig. 7. The grid of the trihedral was oriented horizontally and vertically, sequentially and the distance from it to the antenna array is 0.9 m. The reflected signal was recorded by the two receiving Vivaldi antennas.

From (7) we calculated the two cross-talk parameters, i.e., $\delta_1 = 1.99 - j0.71$ and $\delta_2 = -5.59 - j0.86$, as well as the channel imbalance parameter as $f = 0.27 - j0.19$. Then, these parameters are input into (8) for polarimetric calibration of the hybrid GPR antenna array.

Then, a laboratory experiment was carried out in a sand pit to further verify the accuracy of the hybrid polarimetric GPR system and the proposed method for estimating the orientation angle of a buried elongated object. A metal rebar, which has a diameter of 8 mm and a length of 1.2 m, was buried at a depth of about 15 cm in dry sand at five different orientation angles relative to the GPR survey line. The antenna array is placed at a height of 5 cm above the sand, as illustrated in Fig. 8. Fig. 9 shows the experimental setup. The antenna array was amounted onto a three-dimensional scanning system. GPR signal was recorded along a 1.3 m survey line at a step of 1 cm. The metal rebar was sequentially buried in the sand at an orientation angle of 25.6°, 61.9°, 87.9°, 123.8° and 147.2° with respect to the survey line. The actual orientation angle was estimated by a simple distance measurement with the Pythagorean equation.

The recorded GPR images after pre-processing are shown in Fig. 10(a)–(f) and the migrated ones are shown in Fig. 10(f)–(j).
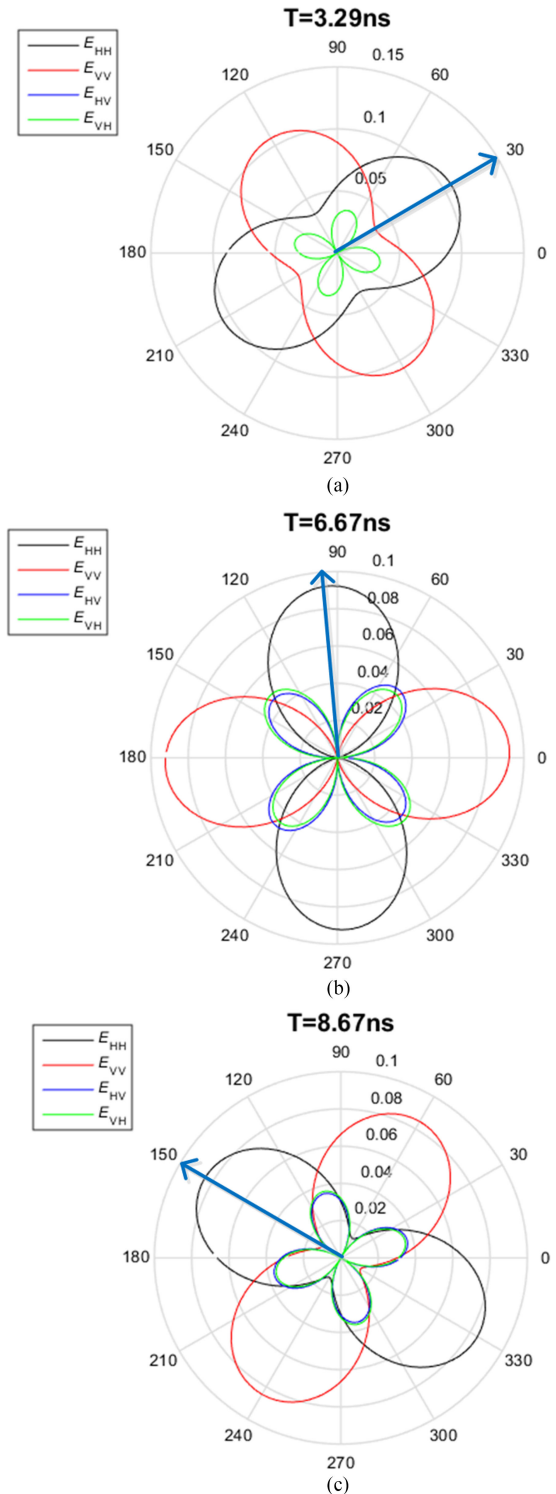

Fig. 6. Polar diagram illustrating the reflection amplitude in four different polarization channels after the polarization rotation of (a) the first rebar, (b) the second rebar, and (c) the third one.

Due to the limited space, only data recorded in the VV channel after polarimetric decomposition and calibration are shown. After migration, the hyperbolic signature of the buried rebar has been focused, especially for the third one with an orientation angle of nearly 90° with respect to the survey direction. The
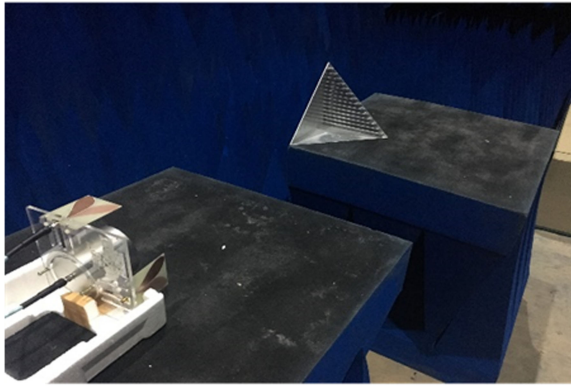
(a)
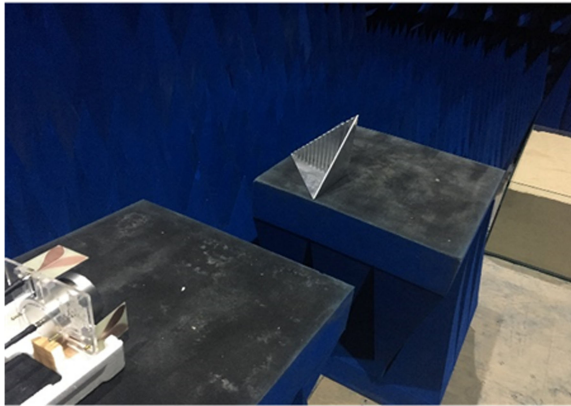
(b)

Fig. 7. Photos illustrating the calibration experiment by a gridded trihedral with two different orientation, i.e., (a) horizontal gridded trihedral1 with $\beta = 90°$ and $\alpha = 0°$ ($gt1$), and (b) vertical gridded trihedral with $\beta = 0°$ and $\alpha = 0°$ ($gt2$).
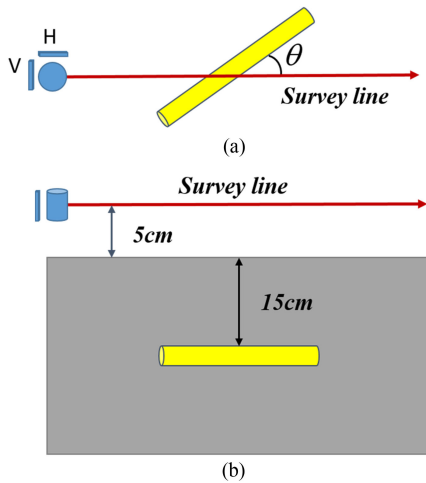

(a)

(b)

Fig. 8. Geometry of the laboratory experimental setup. (a) Plan view. (b) Vertical section.

migrated images of other rebars are less focused, because the rebar has a longer cross section in the vertical sensing plane. Since the orientation angle estimation becomes very unstable for small amplitude in noisy data [8], the orientation angles are evaluated at strong reflection points, at which the amplitude of the reflection signal in the VV channel is larger than
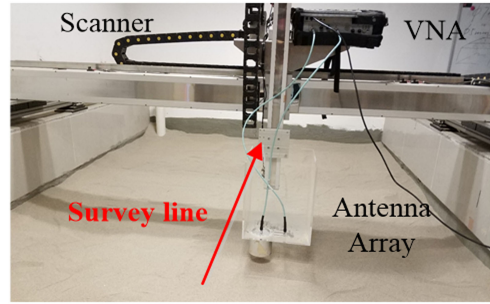
Fig. 9. Photo of the laboratory experiment using the proposed hybrid dual-polarimetric GPR system. The metal rebar was buried at a depth of 15 cm in the sand.
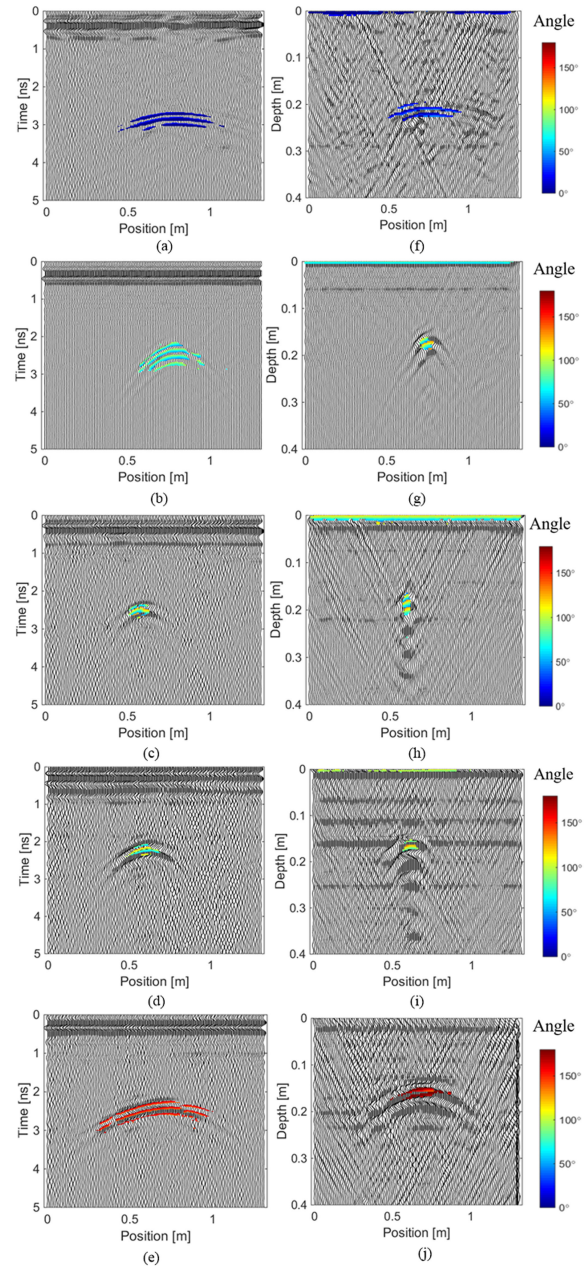

Fig. 10. Recorded GPR profiles from the buried rebar at the direction of (a) 25.6°, (b) 61.9°, (c) 87.9°, (d) 123.8°, and (e) 147.2°. Panels (f–j) show the migrated profiles with the corresponding angles. The estimated orientation angle of the buried rebar is visualized by a color code.

TABLE I
ORIENTATION ANGLES AND THE CORRESPONDING ERRORS OF THE BURIED METAL REBARS IN THE LABORATORY EXPERIMENT

Real angle	Before migration		After migration	
	Estimated angle	Error	Estimated angle	Error
25.6°	22.1°	3.5° (13.7%)	26.4°	0.8° (3.1%)
61.9°	67.2°	5.3° (8.6%)	64.9°	3.0° (4.9%)
87.9°	82.3°	5.6° (6.4%)	84.5°	3.4° (3.9%)
123.8°	119.8°	4.0° (3.2%)	124.9°	1.1° (0.9%)
147.2°	154.5°	7.3° (5.0%)	148.8°	1.6° (1.1%)

70% of the strongest one. From the relative phases of the signals in the four decomposed polarimetric channels at those points, we can estimate the orientation angles using the Alford rotation method. The averaged value is obtained as an output for each detected rebar and the results are given in Table I. We can see that the estimated orientation angles have high accuracy. The maximum relative error of the estimated orientation angle of the buried rebar from the GPR image before migration is less than 14%, and that from the migrated GPR images is less than 5%.

VI. CONCLUSION AND DISCUSSION

In this paper, a hybrid dual-polarization GPR system is employed to detect a subsurface elongated target. This system is composed of a circularly polarized transmitting antenna and two linearly polarized receiving antennas. A polarimetric calibration experiment using a gridded trihedral is conducted to reduce the channel imbalance and cross talk between the two receiving channels. A full-polarimetric scattering matrix can be extracted from GPR reflection signals recorded in the two receiving channels. From the calibrated scattering matrix of the subsurface reflection signal, an improved algorithm based on the Alford rotation transformation is applied to estimate the orientation angle of a buried elongated target with respect to the survey direction. The results of the numerical test validate that the proposed algorithm can estimate the orientation angle of a subsurface elongated target with a high accuracy, and the 90° ambiguity of the estimated angle has been eliminated. From the laboratory experiments, we can find that the orientation direction of a metal rebar buried in sand can be accurately estimated. The maximum relative error of the estimated orientation angle of the buried rebar from the GPR image before migration is less than 14%, and that from the migrated GPR images is less than 5%. Migration can not only focus the hyperbolic reflection from the buried elongated object, but also improve the accuracy of the orientation estimation. It is concluded that radar polarimetry can provide richer information than single-polarization GPR, which provides a reliable approach for orientation estimation of a subsurface elongated object.

There are some limitations of the proposed technique for orientation estimation. It only works for buried conductive cylinders with a diameter that is small compared to wavelength. When the diameter of a subsurface cylinder is larger than the nominal wavelength of GPR, the depolarization capacity of the cylinder

is decreased [6] and the orientation estimation method may be inapplicable. The technique will also produce incorrect results for small diameter plastic cylinders, since the reflection is very weak and overwhelmed by noise and/or clutter.

REFERENCES

[1] P. Kaur, K. J. Dana, F. A. Romero, and N. Gucunski, "Automated GPR rebar analysis for robotic bridge deck evaluation," *IEEE Trans. Cybern.*, vol. 46, no. 10, pp. 2265–2276, Oct. 2016.

[2] H. Liu, J. Zhao, and M. Sato, "A hybrid dual-polarization GPR system for detection of linear objects," *IEEE Antennas Wireless Propag. Lett.*, vol. 14, pp. 317–320, 2015.

[3] A. Benedetto, F. Tosti, L. Bianchini Ciampoli, and F. Damico, "GPR applications across engineering and geosciences disciplines in Italy: A review," *IEEE J. Sel. Topics Appl. Earth Obs. Remote Sens.*, vol. 9, no. 7, pp. 2952–2965, Jul. 2016.

[4] G. P. Tsoflias, J. Van Gestel, P. L. Stoffa, D. D. Blankenship, and M. Sen, "Vertical fracture detection by exploiting the polarization properties of ground-penetrating radar signals," *Geophysics*, vol. 69, no. 3, pp. 803–810, 2004.

[5] V. R. N. Santos and F. L. Teixeira, "Study of time-reversal-based signal processing applied to polarimetric GPR detection of elongated targets," *J. Appl. Geophys.*, vol. 139, pp. 257–268, Apr. 2017.

[6] S. J. Radzevicius and J. J. Daniels, "Ground penetrating radar polarization and scattering from cylinders," *J. Appl. Geophys.*, vol. 45, no. 2, pp. 111–125, Sep. 2000.

[7] A. P. Annan, S. W. Cosway, and T. DeSouza, "Application of GPR to map concrete to delineate embedded structural elements and defects," in *Proc. 9th Int. Conf. Ground Penetrating Radar*, 2002, pp. 359–364.

[8] A. Villela and J. M. Romo, "Invariant properties and rotation transformations of the GPR scattering matrix," *J. Appl. Geophys.*, vol. 90, pp. 71–81, 2013.

[9] J. P. Van Gestel and P. L. Stoffa, "Application of alford rotation to ground-penetrating radar data," *Geophysics*, vol. 66, no. 6, pp. 1781–1792, 2001.

[10] M. Lualdi and F. Lombardi, "Combining orthogonal polarization for elongated target detection with GPR," *J. Geophys. Eng.*, vol. 11, no. 5, 2014, Art. no. 055006.

[11] C. C. Chen, M. B. Higgins, K. O'Neill, and R. Detsch, "UWB fully-polarimetric GPR classification of subsurface unexploded ordnance," *IEEE Trans. Geosci. Remote Sens.*, vol. 39, no. 6, pp. 1221–1230, Jun. 2001.

[12] Z. Zeng, J. Li, L. Huang, X. Feng, and F. Liu, "Improving target detection accuracy based on multipolarization MIMO GPR," *IEEE Trans. Geosci. Remote Sens.*, vol. 53, no. 1, pp. 15–24, Jan. 2015.

[13] Y. Yu, C.-C. Chen, X. Feng, and C. Liu, "Modified entropy-based fully polarimetric target classification method for ground penetrating radars (GPR)," *IEEE J. Sel. Topics Appl. Earth Obs. Remote Sens.*, vol. 10, no. 10, pp. 4304–4312, Oct. 2017.

[14] T.-H. Liu and J. M. Mendel, "Azimuth and elevation direction finding using arbitrary array geometries," *IEEE Trans. Signal Process.*, vol. 46, no. 7, pp. 2016–2065, Jul. 1998.

[15] P. Farinelli and F. Roth, "Frequency domain analysis of the polarimetric ground penetrating radar response of landmines and minelike targets," *Proc. SPIE*, vol. 5089, pp. 437–447, 2003.

[16] S. J. Seol, J. H. Kim, Y. Song, and S. H. Chung, "Finding the strike direction of fractures using GPR," *Geophys. Prospecting*, vol. 49, no. 3, pp. 300–308, 2001.

[17] P. Capizzi and P. L. Cosentino, "GPR multi-component data analysis," *Near Surf. Geophys.*, vol. 6, no. 2, pp. 87–95, 2008.

[18] J. J. Van Zyl, "Calibration of polarimetric radar images using only image parameters and trihedral corner reflector responses," *IEEE Trans. Geosci. Remote Sens.*, vol. 28, no. 3, pp. 337–348, May 1990.

[19] X. Feng, L. Zou, Q. Lu, C. Liu, W. Liang, and Z. S. Zhou, "Calibration with high-order terms of polarimetric GPR," *IEEE J. Sel. Topics Appl. Earth Obs. Remote Sens.*, vol. 5, no. 3, pp. 717–722, Jun. 2012.

[20] J. Chen and S. Quegan, "Calibration of spaceborne CTLR compact polarimetric low-frequency SAR using mixed radar calibrators," *IEEE Trans. Geosci. Remote Sens.*, vol. 49, no. 7, pp. 2712–2723, Jul. 2011.

[21] P. Pincus, M. Preiss, A. S. Goh, and D. Gray, "Polarimetric calibration of circularly polarized synthetic aperture radar data," *IEEE Trans. Geosci. Remote Sens.*, vol. 55, no. 12, pp. 6824–6839, Dec. 2017.

[22] E. Pancera, T. Zwick, and W. Wiesbeck, "Full polarimetric time domain calibration for UWB radar systems," in *Proc. Eur. Radar Conf.*, 2009, pp. 105–108.

[23] M. Lavalle, B. Rosich, T. Ainsworth, E. Pottier, and D. Solimini, "Calibration of dual-pol arimetric C-band SAR data: A possible approach for Sentinel-1," in *Proc. PollnSAR Workshop*, 2009, pp. 26–31.

[24] R. M. Alford and P. C. Amoco, "Shear data in presence of azimuthal anisotropy: Dilley, Texas," in *Proc. 56th Annu. Int. Meeting Soc. Exploration Geophys.*, 1968, pp. 476–479.

[25] H. Liu and M. Sato, "Determination of the phase center position and delay of a Vivaldi antenna," *IEICE Electron. Express*, vol. 10, no. 21, pp. 1–7, 2013.

[26] L. Zhou, C. Huang, and Y. Su, "A fast back-projection algorithm based on cross correlation for GPR imaging," *IEEE Geosci. Remote Sens. Lett.*, vol. 9, no. 2, pp. 228–232, Mar. 2012.

Hai Liu (S'11–M'13) received the B.E. and M.E. degrees in civil engineering from Tongji University, Shanghai, China, in 2007 and 2009, respectively, and the Ph.D. degree in environmental studies from Tohoku University, Sendai, Japan, in 2013.

From April 2013 to March 2014, he was with the Center for Northeast Asian Studies, Tohoku University, as a Research Fellow. From July 2014 to July 2017, he was an Assistant Professor with the Institute of Electromagnetics and Acoustics, Xiamen University, Xiamen, China. He is currently an Associate Professor with the School of Civil Engineering, Guangzhou University, Guangzhou, China. His current research interests include development of ground-penetrating radar systems and algorithms for a wide variety of applications, such as nondestructive testing in civil engineering, environmental monitoring, archeological investigation, and lunar exploration.

Dr. Liu received the Young Researcher Award of the 14th International Conference on Ground Penetrating Radar in 2012 and the Excellent Paper Award of the IET International Radar Conference in 2013.

**Xiaoyun Huang**, photograph and biography not available at the time of publication.
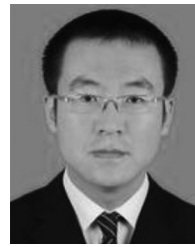
Feng Han received the B.S. degree in electronic science from Beijing Normal University, Beijing, China, in 2003, the M.S. degree in geophysics from Peking University, Beijing, in 2006, and the Ph.D. degree in electrical engineering from Duke University, Durham, NC, USA, in 2011.

He is currently an Assistant Professor with the Institute of Electromagnetics and Acoustics, Xiamen University, Xiamen, China. His research interests include ionosphere remote sensing by radio atmospherics, electromagnetic full-wave inversion by integral equations, subsurface imaging, and the design of an electromagnetic detection system.

Jie Cui, photograph and biography not available at the time of publication.

Billie F. Spencer, photograph and biography not available at the time of publication.
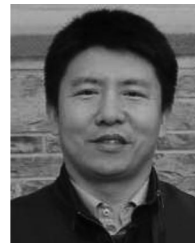
Xiongyao Xie received the bachelor's degree in applied geophysics from the Changchun College of Geology in 1995, the master's degree in applied geophysics from Tongji University in 1998, and the Ph.D. degree in geotechnical engineering from Tongji University in 2001.

He is currently a Professor with the Department of Geotechnical Engineering, Tongji University, Shanghai, China. He has authored or coauthored more than 100 publications in peer-referred journals, conference proceedings, and technical reports. His current research focuses on non-destructive test, risk evaluation, and disaster reduction in tunnel and underground space.